Polym. Bull. (2013) 70:3143–3153
DOI 10.1007/s00289-013-1013-1

ORIGINAL PAPER

Using Agrawal integral equation and thermogravimetric analysis (TGA) to study the pyrolysis kinetics of nanocomposites of polybenzoxazine and exfoliated montmorillonite from a mono-functionalized azide polyhedral oligomeric silsesquioxane and click chemistry

Hui-Wang Cui · Shiao-Wei Kuo

Received: 20 May 2013 / Revised: 29 July 2013 / Accepted: 5 August 2013 / Published online: 13 August 2013

Abstract In this study, an exfoliated montmorillonite was prepared through click chemistry from a singly azido-functionalized polyhedral oligomeric silsesquioxane derivative and a montmorillonite intercalated with propargyldimethylstearylammonium bromide. This exfoliated montmorillonite was then introduced into a benzoxazine matrix—prepared from paraformaldehyde, aniline, and phenol—to form polymer/exfoliated clay nanocomposites. Thermogravimetric analysis revealed that the pyrolysis kinetics had a close relationship with the structure of montmorillonite, the assembly process, the anchoring effect, the compatibility of the polymer and intercalator, and the char yield. The polymer/exfoliated clay nanocomposites had a same mechanism function, and the kinetic compensation effect equations revealed the pyrolysis essences.

Keywords Nanocomposites · Polybenzoxazine · Montmorillonite · POSS · Pyrolysis kinetics

Introduction

Polybenzoxazines exhibit many unique properties, such as near-zero volume changes upon polymerization with high mechanical integrity, low water absorption

Electronic supplementary material The online version of this article (doi:10.1007/s00289-013-1013-1) contains supplementary material, which is available to authorized users.

H.-W. Cui · S.-W. Kuo
Department of Materials and Optoelectronic Science, National Sun Yat-Sen University, Kaohsiung 804, Taiwan

H.-W. Cui (✉)
Institute of Scientific and Industrial Research, Osaka University, Ibaraki, Osaka 565-0047, Japan
e-mail: cuihuiwang@hotmail.com

in water at room temperature, surprisingly high glass transition temperatures, rapid development of their physical and mechanical properties during the polymerization process, very high char yields, low surface energies, etc. [1–7]. Therefore, polybenzoxazines have been studied widely ever since they were first reported [8], and various related applications are also appearing gradually [9–14]. To further improve the physical properties of polybenzoxazines, one of the most important technologies is to manufacture the nanocomposites through blending with other polymers or nanofillers [15–17]. These nanocomposites can impart polybenzoxazines with excellent processability and superb mechanical properties, without forming volatile species. Although many reports describe nanocomposites manufactured through the incorporation of clay into polybenzoxazines, in those cases the clays were merely intercalated and dispersed in the polymeric matrix with a layered or lamellar structure [18–22].

In this study, we used polyhedral oligomeric silsesquioxane (POSS) nanocomposites to improve the exfoliation of clay incorporated in a polybenzoxazine. POSS derivatives, unlike most silicones or fillers, are cage-like molecules presenting organic substituents on their outer surfaces, making them compatible or miscible with most polymers. These functional groups can be designed to be either non-reactive or reactive [23–27]. Therefore, after intercalating propargyl dimethylstearylammonium bromide (PDS) between the layers of montmorillonite (MMT) to form intercalated montmorillonite (In-MMT), we introduced a mono-functionalized azide-POSS derivative (N_3-POSS) to undergo click reactions with the acetylenic intercalator units, resulting in the MMT exfoliated into nanoparticles in the form of single sheets or layers (Scheme 1) [28]. We then incorporated this exfoliated montmorillonite (Ex-MMT) into the Pa-type benzoxazine (3-phenyl-3,4-dihydro-2H-benzoxazine) monomer—derived from paraformaldehyde, aniline, and phenol—to form exfoliated polybenzoxazine nanocomposites [29], the pyrolysis kinetics of which we investigated using Agrawal integral equation and thermogravimetric analysis (TGA).

Experiments

Samples

The pristine montmorillonite (MMT) was purchased from Nanocor (USA). The Pa-type benzoxazine (3-phenyl-3,4-dihydro-2H-benzoxazine) monomer, In-MMT, and Ex-MMT were prepared according to previously reported procedures. The Pa-type benzoxazine monomer was prepared from paraformaldehyde, aniline, and phenol [12, 30]. As Scheme 1a shows, In-MMT was prepared from pristine MMT and PDS [28], and Ex-MMT from In-MMT and N_3-POSS through click chemistry [28, 31–33]. PDS and N_3-POSS underwent a click reaction with copper (I) bromide (CuBr) and *N*,*N*,*N*,*N*,*N*-pentamethyldiethylenetriamine (PMDETA) as catalysts (Scheme 1b).

The polybenzoxazine/clay nanocomposites were prepared as the following processes [29]: Pa-type benzoxazine monomer was mixed with MMT, In-MMT, or Ex-MMT with vigorously stirring until the sample became homogeneous; the

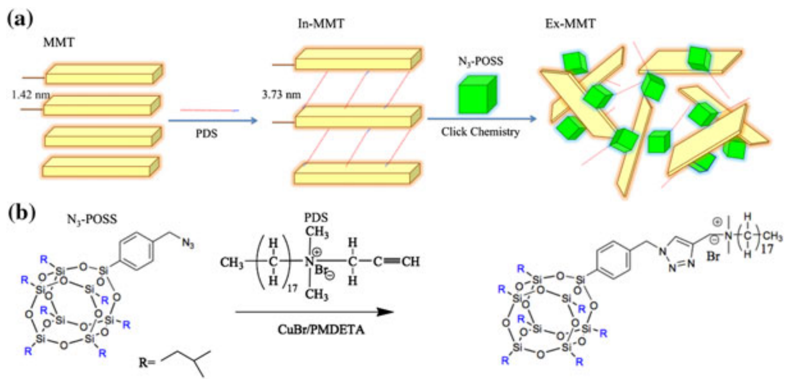

Scheme 1 **a** Preparation of In-MMT and Ex-MMT, and **b** click reaction of PDS with mono-functionalized azide POSS

sample was then placed in a natural oven and cured at 140 °C for 3 h, 160 °C for 3 h, and then 200 °C for 4 h under a heating rate of 2 °C·min^{-1}; BM was formed from Pa polybenzoxazine and pristine MMT; BIM from Pa polybenzoxazine and In-MMT; and BEM from Pa polybenzoxazine and Ex-MMT (Table 1); the weight ratio of MMT or In-MMT to Pa polybenzoxazine was fixed at 5 %; those of Ex-MMT to Pa polybenzoxazine were 1, 3, 5, 7, 10, 30, and 50 %, named BEM-A, BEM-B, BEM-C, BEM-D, BEM-E, BEM-F, and BEM-G, respectively.

Characterization

The thermal degradation of the samples was measured using a TA Q-50 thermogravimetric analyzer operated under an atmosphere of pure N_2. The sample (ca. 7 mg) was placed in a Pt cell and heated at the rate of 20 °C·min^{-1} from 30 to 800 °C under a N_2 flow rate of 60 mL·min^{-1}.

Table 1 Compositions of polybenzoxazine/clay nanocomposites

	BM	BIM	BEM-A	BEM-B	BEM-C	BEM-D	BEM-E	BEM-F	BEM-G
Pa	5 g	5 g	5 g	5 g	5 g	5 g	5 g	5 g	5 g
MMT	0.25 g	–	–	–	–	–	–	–	–
In-MMT	–	0.25 g	–	–	–	–	–	–	–
Ex-MMT	–	–	0.05 g	0.15 g	0.25 g	0.35 g	0.50 g	1.50 g	2.50 g

Results and discussion

There were many reports on the thermal properties of polybenzoxazines and their composites [34–41], but none of them involved the pyrolysis kinetics, and the related influencing factors in this aspect were not investigated, either. Therefore, in this study, the pyrolysis kinetics of nanocomposites of BEM was the point.

In the pyrolysis kinetics, the mechanism function of $G\,(a)$ is

$$G\,(a) = \frac{A}{\beta}\int_{T_0}^{T} \mathrm{e}^{-\frac{E}{RT}}\mathrm{d}T$$

The Agrawal approximate equation is [42, 43]

$$\int_{T_0}^{T} \mathrm{e}^{-\frac{E}{RT}}\mathrm{d}T = \frac{RT^2}{E}\left[\frac{1-\left(\frac{RT}{E}\right)}{1-5\left(\frac{RT}{E}\right)^2}\right]\mathrm{e}^{-\frac{E}{RT}}$$

Combining the above two equations together, the Agrawal integral equation is

$$\ln\left[\frac{G\,(a)}{T^2}\right] = \ln\left\{\frac{AB}{\beta E}\left[\frac{1-\left(\frac{RT}{E}\right)}{1-5\left(\frac{RT}{E}\right)^2}\right]\right\} - \frac{E}{RT}$$

For the general reaction temperatures and most of E, the relationship among E, R, and T are

$$\frac{E}{RT} > > 1, \quad 1-\left(\frac{RT}{E}\right) \approx 1, \text{ and } 1-5\left(\frac{RT}{E}\right)^2 \approx 1.$$

The Agrawal integral equation is simplified as

$$\ln\left[\frac{G\,(a)}{T^2}\right] = \ln\left(\frac{AR}{\beta E}\right) - \frac{E}{RT}$$

The relationship between $\ln\left[\frac{G\,(a)}{T^2}\right]$ and $\frac{1}{T}$ will be linear with a suitable $G\,(a)$, and then E can be calculated from the linear slope and A from the linear intercept. In the above equations, T (K) is the temperature, R is the universal gas constant of 8.314 J·(mol·K)$^{-1}$, β is the heating rate, E (kJ·mol^{-1}) is the active energy, A (min^{-1}) is the frequency factor, and a is the relative weight loss calculated by

$$a = \frac{m_i - m_T}{m_i - m_f}$$

Where m_i (g) is the initial weight, m_f (g) is the final weight, and m_T (g) is the weight at T.

According to the simplified Agrawal integral equation, T and a in the pyrolysis phases of Pa polybenzoxazine, BM, BIM, and BEM (Fig. 1) were linear fit using a trial-and-error method [44–47], as shown in Table S1–S10. On the basis of the linearly dependent coefficient (r), the pyrolysis kinetics of Pa polybenzoxazine, BM, BIM, and BEM was obtained, as shown in Table 2.

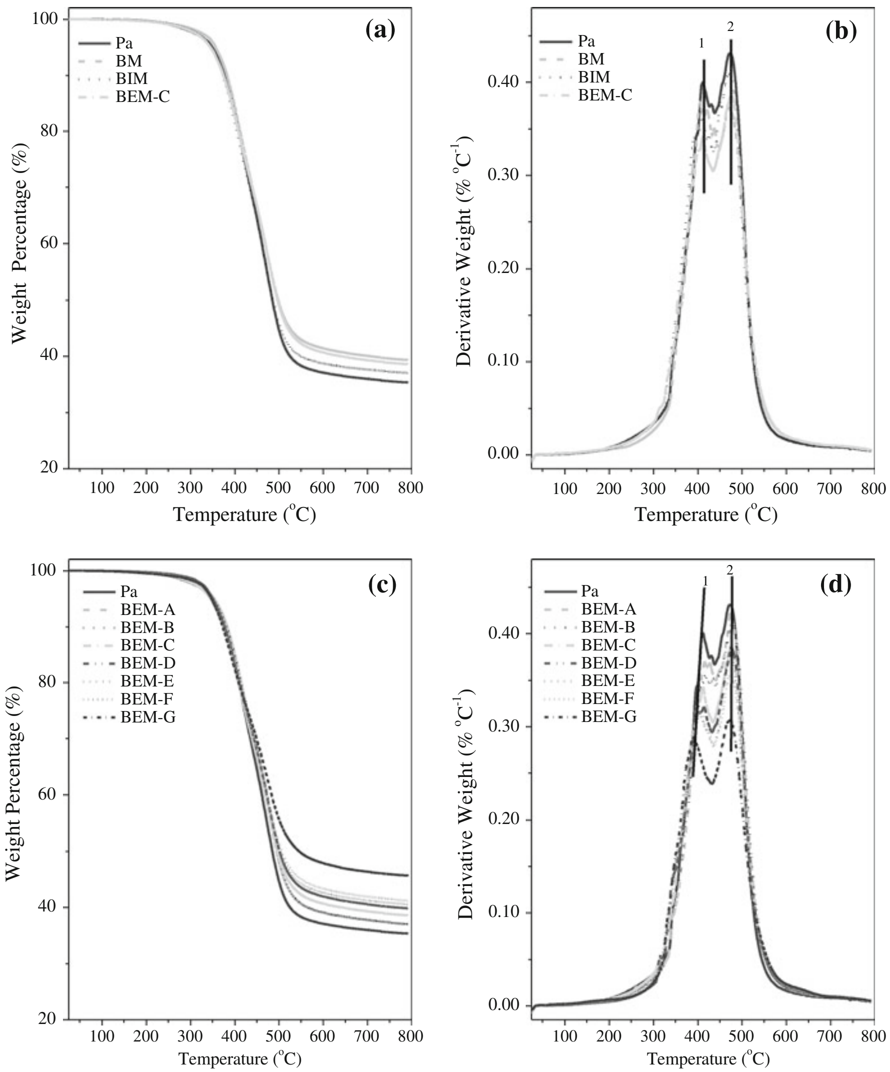

Fig. 1 TGA data revealing the (**a**, **c**) weight percentages and (**b**, **d**) derivative weights of Pa, BM, BIM, BEM-C, and Pa polybenzoxazine samples containing various contents of Ex-MMT (BEM)

In these kinetic parameters, $G(a)$ is the kinetics mechanism function to illustrate the pyrolysis process. If the $G(a)$ is different, the linear fit equation, r, E, and A definitely different also. As Table 2 shows, the $G(a)$ was the same for Pa polybenzoxazine, BM, BIM, and BEM. All was Zhuralev-Lesokin-Tempelman equation with a mechanism of three-dimensional diffusion, 3D, which indicated that the pyrolysis kinetics happened mainly on the polymeric matrix of Pa polybenzoxazine, and the pristine MMT, In-MMT, and Ex-MMT did not have any effect on this aspect.

Table 2 Pyrolysis kinetics of Pa, BM, BIM, and BEM

	$G(a)$	E (kJ·mol^{-1})	A (min^{-1})		$G(a)$	E (kJ·mol^{-1})	A (min^{-1})
Pa	$\left[(1-a)^{-\frac{1}{3}}-1\right]^2$	268.57	4.06×10^{18}	BEM-C	$\left[(1-a)^{-\frac{1}{3}}-1\right]^2$	247.92	1.14×10^{17}
BM	$\left[(1-a)^{-\frac{1}{3}}-1\right]^2$	267.96	3.43×10^{18}	BEM-D	$\left[(1-a)^{-\frac{1}{3}}-1\right]^2$	238.24	2.47×10^{16}
BIM	$\left[(1-a)^{-\frac{1}{3}}-1\right]^2$	257.89	9.93×10^{17}	BEM-E	$\left[(1-a)^{-\frac{1}{3}}-1\right]^2$	234.77	1.47×10^{16}
BEM-A	$\left[(1-a)^{-\frac{1}{3}}-1\right]^2$	269.51	3.70×10^{18}	BEM-F	$\left[(1-a)^{-\frac{1}{3}}-1\right]^2$	234.71	1.47×10^{16}
BEM-B	$\left[(1-a)^{-\frac{1}{3}}-1\right]^2$	260.15	6.80×10^{17}	BEM-G	$\left[(1-a)^{-\frac{1}{3}}-1\right]^2$	215.46	4.76×10^{14}

E is the required minimum energy of the molecules from a reactant state to an activated state in a chemical reaction. In the pyrolysis, it is the different energy between the onset point and the offset point. A is a constant determined by the reaction essence and does not have any relationship to the reaction temperature and concentration in the system. The E and A always have a same variation trend. Figure 1a shows the TGA traces of Pa polybenzoxazine, BM, BIM, and BEM-C. The char yield of Pa polybenzoxazine was 35.4 wt%. Because of the presence of inorganic MMT, the char yield of BM increased to 39.4 wt%. Although the char yield of BIM at 37.1 wt% was higher than that of Pa polybenzoxazine, it was lower than that of BM because the organic intercalator, propargyldimethylstearylammonium bromide, had entered into the MMT layers. The char yield of BEM-C (38.62 %) was lower than that of BM, but higher than those of Pa polybenzoxazine and BIM, because of the click reactions that had occurred between the propargyl-containing intercalator and the mono-functionalized azide POSS in the MMT layers [29]. Therefore, the order of their char yields was Pa polybenzoxazine < BIM < BEM-C < BM. However, the E and A for Pa polybenzoxazine, BM, BIM, and BEM-C did not show a corresponding variation. Instead, the order of their E and A was Pa polybenzoxazine>BM>BIM>BEM-C, which showed the E and A had a close relationship not only with their char yields, but also with their structures, especially with regard to the degree of dispersion of pristine MMT, In-MMT, and Ex-MMT in the polymeric matrix. The pristine MMT had a lamellar structure, In-MMT was an intercalated nanocomposite, and Ex-MMT was an exfoliated nanocomposite; therefore, each was dispersed in the polybenzoxazine matrix in a different state [28, 29]. The primary building blocks of the nanodomains of pristine MMT consisted of an assembly of many lamellae (lamella multiples), arranged compactly and densely in a certain direction. In-MMT had a similar, or possibly even the same, layered morphology as that of pristine MMT, but the arrangement was not as compact or dense as that of pristine MMT. Ex-MMT did not have a lamellar structure; the MMT had been exfoliated into nanoparticles, either single sheets or layers, as a result of the click reactions of the cage-like POSS nanoparticles. These single sheets or layers were dispersed randomly and freely in the polymeric matrix and formed different dispersion states, such as so-called "random dispersion" and "island dispersion". Moreover, the random and island dispersions always appeared together in the form of the mixed dispersion. The Ex-MMT-based nanocomposites often contained more than one dispersion of the exfoliated single sheets or layers. During the intercalation process leading to the formation of In-MMT, the exfoliation and click reactions leading to Ex-MMT, and the strong stirring in the preparation of BEM, the MMT was exfoliated into nanoparticles in the form of thin solid layers, elementary particles, or aggregates of the two. The Ex-MMT nanoparticles and the polybenzoxazine chains also underwent an assembly process during the strong stirring used in the preparation of BEM. The different charges of the components led to the formation of ionic bonds between them; this assembly process not only had a further exfoliation effect on the Ex-MMT nanoparticles but also anchored these exfoliated single sheets or layers with polybenzoxazine chains through physical crosslinking. In addition, the Ex-MMT nanoparticles interacted also with the polybenzoxazine chains indirectly as a result of the latter's compatibility with propargyldimethylstearylammonium bromide. In other words, the structure of MMT, the assembly process, the anchoring effect, the compatibility of the polymer and intercalator, and the char yield all combined so that the BM, BIM, and BEM-C systems possessed different values of E and A displayed in Table 2.

Figure 1c mainly shows the TGA traces of BEM, which was composited of Pa polybenzoxazine and Ex-MMT with various contents. BEM had similar, even same structures, so the E and A were determined only by the char yield. As Fig. 1c and Table 2 shows, the char yield order was BEM-A < BEM-B < BEM-C < BEM-D < BEM-E < BEM-F < BEM-G, while that of the E and A was BEM-A > BEM-B > BEM-C > BEM-D > BEM-E > BEM-F > BEM-G.

The factors described above also influenced the reaction rate constant (k) calculated by Arrhenius equation [48–51]:

$$k = Ae^{-\frac{E}{RT}}$$

k is related closely to the reaction temperature, reaction medium (or solvent), catalyst, and so on, even to the shape and characteristics of reactors. Thus, the k (k_1 and k_2) at the temperatures of Peak 1 (T_1) and Peak 2 (T_2) marked in Fig. 1b and d varied accordingly with the variation of E, A, T_1, and T_2, as shown in Table 3.

Table 3 Derivative weight data of Pa, BM, BIM, and BEM

	Temperature (°C)		k (min^{-1})			Temperature (°C)		k (min^{-1})	
	T_1	T_2	k_1	k_2		T_1	T_2	k_1	k_2
Pa	414.5	475.0	1.61×10^{-2}	7.19×10^{-1}	BEM-C	413.6	475.7	1.58×10^{-2}	5.80×10^{-1}
BM	406.7	470.5	8.84×10^{-3}	5.16×10^{-1}	BEM-D	415.2	477.3	2.06×10^{-2}	6.45×10^{-1}
BIM	411.6	475.4	2.11×10^{-2}	1.00	BEM-E	404.1	477.0	1.15×10^{-2}	6.59×10^{-1}
BEM-A	421.5	474.5	2.00×10^{-2}	5.47×10^{-1}	BEM-F	403.0	474.4	1.08×10^{-2}	5.84×10^{-1}
BEM-B	418.4	478.8	1.52×10^{-2}	5.76×10^{-1}	BEM-G	390.6	476.1	5.26×10^{-3}	4.53×10^{-1}

Temperature and k were the values at Peak 1 and Peak 2 marked in Fig. 1b and d

Table 4 Kinetic compensation effect equations of Pa, BM, BIM, and BEM

	Kinetic compensation effect equation		Kinetic compensation effect equation
Pa	ln$A$ = 0.0002E − 1.8951	BEM-C	ln$A$=0.0002E − 2.0574
BM	ln$A$ = 0.0002E − 1.9003	BEM-D	ln$A$=0.0002E − 2.0607
BIM	ln$A$ = 0.0002E − 1.9728	BEM-E	ln$A$=0.0002E − 2.0913
BEM-A	ln$A$ = 0.0002E − 1.9277	BEM-F	ln$A$=0.0002E − 2.1071
BEM-B	ln$A$ = 0.0002E − 2.0265	BEM-G	ln$A$=0.0002E − 2.3789

The kinetic compensation effect is often used also in the kinetics. It indicates a linear relationship between ln$A$ and E that A compensates to the change of E partly [45, 52–56]:

$$\ln A = KE + Q,$$

where K and Q are the kinetic compensation effect parameters calculated from the linear fit between E and A.

Table 4 shows the kinetic compensation effect equations of Pa polybenzoxazine, BM, BIM, and BEM. The K all was the same at 0.0002, which coincided well with the kinetics mechanism function of $G(a)$ and indicated also that the pyrolysis happened mainly on the polymeric matrix of Pa polybenzoxazine. It can be seen that the order of the Q was Pa polybenzoxazine > BM > BIM > BEM-C and BEM-A > BEM-B > BEM-C > BEM-D > BEM-E > BEM-F > BEM-G, which was similar to their orders of the E and A, showing the Q also had a close relationship with the structure of MMT, the assembly process, the anchoring effect, the compatibility of the polymer and intercalator, and the char yield. Because the K and Q are not affected by experimental factors, the kinetic compensation effect equations can explain the pyrolysis processes and reveal the pyrolysis essences of Pa polybenzoxazine, BM, BIM, and BEM, and also are their theoretical expressions.

Conclusions

In this study, the pyrolysis kinetics of Pa polybenzoxazine, BM, BIM, and BEM was investigated using Agrawal integral equation, which had a close relationship with the structure of MMT, the assembly process, the anchoring effect, the compatibility of the polymer and intercalator, and the char yield. The Pa polybenzoxazine, BM, BIM, and BEM all had a same $G(a)$ of Zhuralev-Lesokin-Tempelman equation and a same kinetic compensation effect parameter of K at 0.0002, indicating that the pyrolysis happened mainly on the polymeric matrix of Pa polybenzoxazine. The kinetic compensation effect equations revealed the pyrolysis essences of Pa polybenzoxazine, BM, BIM, and BEM.

References

1. Ishida H, Allen DJ (1996) Physical and mechanical characterization of near-zero shrinkage polybenzoxazines. J Polym Sci Part B 34:1019–1030
2. Ishida H, Low HY (1997) A study on the volumetric expansion of benzoxazine-based phenolic resin. Macromolecules 30:1099–1106
3. Kanchanasopa M, Yanumet N, Hemvichian K, Ishida H (2001) The effect of polymerization conditions on the density and T_g of bisphenol-A and hexafluoroisopropylidene-cotaining polybenzoxanines. Polym Polym Compos 9:367–375
4. Wang CF, Su YC, Kuo SW, Huang CF, Sheen YC, Chang FC (2006) Low-surface-free-energy materials based on polybenzoxazines. Angew Chem Int Ed 45:2248–2251
5. Kuo SW, Wu YC, Wang CF, Jeong KU (2009) Low surface energy materials through mediated by hydrogen bonding interaction. J Phys Chem C 113:20666–20673
6. Jin L, Agag T, Ishida H (2010) Bis(benzoxazine-maleimide)s as a novel class of high performance resin: synthesis and properties. Eur Polym J 46:354–363
7. Kiskan B, Ghosh NN, Yagci Y (2011) Polybenzoxazine-based composites as high-performance materials. Polym Int 60:167–177
8. Holly FW, Cope AC (1994) Condensation products of aldehydes and ketones with o-aminobenzyl alcohol and o-hydroxybenzylamine. J Am Chem Soc 66:1875–1879
9. Wang CF, Wang YT, Tung PH, Kuo SW, Lin CH, Sheen YC, Chang FC (2006) Fabrication of patterned superhydrophobic polybenzoxazine hybrid surfaces. Langmuir 22:8289–8292
10. Wang CF, Chiou SF, Ko FH, Chen JK, Chou CT, Huang CF, Kuo SW, Chang FC (2007) Polybenzoxazine as a mold-release agent for nanoimprint lithography. Langmuir 23:5868–5871
11. Yang P, Gu Y (2011) Synthesis and curing behavior of a benzoxazine based on phenolphthalein and its high performance polymer. J Polym Res 18:1725–1733
12. Ishida H (2011) In: Ishida H, Agag T (eds.) Handbook of Benzoxazine Resins. Elsevier, Amsterdam, Ch. 1, pp 1–81
13. Wang CF, Wang TF, Liao CS, Kuo SW, Lin HC (2011) Using pencil drawing to pattern robust superhydrophobic surfaces to control the mobility of water droplets. J Phys Chem C 115:16495–16500
14. Baqar M, Agag T, Ishida H, Qutubuddin S (2011) Poly(benzoxazine-courethane)s: a new concept for phenolic/urethane copolymers via onepot method. Polymer 52:307–317
15. Su YC, Kuo SW, Yei DR, Xu HY, Chang FC (2003) Thermal properties and hydrogen bonding in polymer blend of polybenzoxazine/poly(N-vinyl-2-pyrrolidone). Polymer 44:2187–2191
16. Huang JM, Kuo SW, Lee YJ, Chang FC (2007) Synthesis and characterization of a vinyl-terminated benzoxazine monomer and its blends with poly(ethylene oxide). J Polym Sci Part B 45:644–653
17. Kuo SW, Liu WC (2010) Synthesis and characterization of a cured epoxy resin with a benzoxazine monomer containing allyl groups. J Appl Polym Sci 117:3121–3127
18. Sudo A, Kudoh R, Nakayama H, Arima K, Endo T (2008) Selective formation of poly(N, O-acetal) by polymerization of 1,3-benzoxazine and its main chain rearrangement. Macromolecules 41:9030–9034
19. Agag T, Takeichi T (2008) Preparation and cure behavior of organoclay-modified allyl-functional benzoxazine resin and the properties of their nanocomposites. Polym Compos 29:750–757
20. Fu HK, Huang CF, Kuo SW, Lin HC, Yei DR, Chang FC (2008) Effect of an organically modified nanoclay on low-surface-energy materials of polybenzoxazine. Macromol Rapid Commun 29:1216–1220
21. Chozhan CK, Alagar M, Gnanasundaram P (2009) Synthesis and characterization of 1,1-bis(3-methyl-4-hydroxy phenyl)cyclohexane polybenzoxazine–organoclay hybrid nanocomposites. Acta Mater 57:782–794
22. Garea SA, Iovu H, Nicolescu A, Deleanu C (2009) A new strategy for polybenzoxazine–montmorillonite nanocomposites synthesis. Polym Test 28:338–347
23. Chou CH, Hsu SL, Dinakaran K, Chiu MY, Wei KH (2005) Synthesis and characterization of luminescent polyfluorenes incorporating side-chain-tethered polyhedral oligomeric silsesquioxane units. Macromolecules 38:745–751
24. Chou CH, Hsu SL, Yeh SW, Wang HS, Wei KH (2005) Enhanced luminance and thermal properties of poly(phenylenevinylene) copolymer presenting side-chain-tethered silsesquioxane units. Macromolecules 38:9117–9123

25. Song XY, Zhou SZ, Wang YF, Kang WM, Cheng BW (2012) Mechanical and electret properties of polypropylene unwoven fabrics reinforced with POSS for electret filter materials. J Polym Res 19:9812
26. Chandramohan A, Devaraju S, Vengatesan MR, Alagar M (2012) Octakis(dimethylsiloxypropylglycidylether)silsesquioxane (OG-POSS) reinforced 1,1-bis(3-methyl-4-hydroxymethyl) cyclohexane based polybenzoxazine nanocomposites. J Polym Res 19:9903
27. Wang WP, Ding WL, Yu J, Fei M, Tang JY (2012) Synthesis and characterization of a novel POSS/PS composite via ATRP of branched functionalized POSS. J Polym Res 19:9948
28. Cui HW, Kuo SW (2012) Using a polyhedral oligomeric silsesquioxane surfactant and click chemistry to exfoliate montmorillonite. RSC Adv 2:12148–12152
29. Cui HW, Kuo SW (2013) Nanocomposites of polybenzoxazine and exfoliated montmorillonite using a polyhedral oligomeric silsesquioxane surfactant and click chemistry. J Polym Res 20:114
30. Huang KW, Kuo SW (2010) High performance polybenzoxazine nanocomposites containing multifunctional polyhedral oligomeric silsesquioxane (POSS) with allyl groups. Macromol Chem Phys 211:2301–2311
31. Lin YC, Kuo SW (2011) Self-assembly and secondary structures of linear polypeptides tethered to polyhedral oligomeric silsesquioxane nanoparticle through click chemistry. J Polym Sci Part A 49:2127–2137
32. Lin YC, Kuo SW (2012) Synthesis, self-assembly and secondary structures of linear polypeptides graft to polyhedral oligomeric silsesqu ioxane in the side chain through click chemistry. Polym Chem 3:162–171
33. Hu WH, Huang KW, Kuo SW (2012) Heteronucleobase-functionalized benzoxazine: synthesis, thermal properties, and self-assembled structure formed through multiple hydrogen bonding interactions. Polym Chem 3:1546–1554
34. Wang J, Fang X, Wu MQ, He XY, Liu WB, Shen XD (2011) Synthesis, curing kinetics and thermal properties of bisphenol-AP-based benzoxazine. Eur Polym J 47:2158–2168
35. Zhang J, Huang JX, Du W, Huang FR, Du L (2011) Thermal stability of the copolymers of silicon-containing arylacetylene resin and acetylene-functional benzoxazine. Polym Degrad Stabil 96:2276–2283
36. Lin CH, Huang SJ, Wang PJ, Lin HT, Dai SHA (2012) Miscibility, microstructure, and thermal and dielectric properties of reactive blends of dicyanate ester and diamine-based benzoxazine. Macromolecules 45:7416–7466
37. Ran QC, Zhang DX, Zhu RQ, Gu Y (2012) The structural transformation during polymerization of benzoxazine/FeCl3 and the effect on the thermal stability. Polymer 53:4119–4127
38. Yang P, Gu Y (2012) A novel benzimidazole moiety-containing benzoxazine: synthesis, polymerization, and thermal properties. J Polym Sci Part A 50:1261–1271
39. Yang P, Wang XF, Gu Y (2012) Copolymers of phenolphthalein-aniline-based benzoxazine and biphenyl epoxy: curing behavior and thermal and mechanical properties. J Polym Res 19:9901
40. Liu YF, Wang M, Zhang HL, Zhao SS, Run MT (2013) Synthesis, polymerization, and thermal properties of benzoxazine based on bisphenol-S and allylamine. Polym Adv Technol 24:157–163
41. Vengatesan MR, Devaraju S, Kannaiyan D, Song JK, Alagar M (2013) Ultrasound-assisted synthesis of benzoxazine monomers: thermal and mechanical properties of polybenzoxazines. Polym Int 62:127–133
42. Agrawal RK (1987) A new equation for modeling nonisothermal kinetics. J Therm Anal 32:149–156
43. Sladkov IB (2002) Calculating density of molecular liquids using Agrawal-Thodos equation. Russ J Appl Chem 75:1770–1773
44. Halab-Kessira L, Ricard A (1999) Use of the trial and error method for the optimization of the graft copolymerization of a cationic monomer onto cellulose. Eur Polym J 35:1065–1071
45. Hu RZ, Shi QZ (2001) Thermal analysis kinetics. Science Press, Beijing
46. Woo MW, Daud WRW, Tasirin SM, Talib MZM (2007) Optimization of the spray drying operating parameters-A quick trial-and-error method. Dry Technol 25:1741–1747
47. Taillandier P, Duchene C, Drogoul A (2011) Automatic revision of the control knowledge used by trial and error methods: application to cartographic generalisation. Appl Soft Comput 11:2818–2831
48. Muff S, Caflisch A (2009) ETNA: equilibrium transitions network and Arrhenius equation for extracting folding kinetics from REMD simulations. J Phys Chem B 113:3218–3226
49. Petrowsky M, Frech R (2009) Temperature dependence of ion transport: the compensated Arrhenius equation. J Phys Chem B 113:5996–6000

50. Petrowsky M, Frech R (2010) Salt concentration dependence of the compensated Arrhenius equation for alcohol-based electrolytes. Electrochim Acta 55:1285–1288
51. Sierra CA (2012) Temperature sensitivity of organic matter decomposition in the Arrhenius equation: some theoretical considerations. Biogeochemistry 108:1–15
52. Ruvolo A, Curti PS (2006) Chemical kinetic model and thermodynamic compensation effect of alkaline hydrolysis of waste poly(ethylene terephthalate) in nonaqueous ethylene glycol solution. Ind Eng Chem Res 45:7985–7996
53. Marcilla A, Gomez A, Menargues S, Garcia-Quesada JC (2007) New approach to elucidate compensation effect between kinetic parameters in thermogravimetric data. Ind Eng Chem Res 46:4382–4389
54. Yip K, Ng E, Li CZ, Hayashi JI, Wu HW (2011) A mechanistic study on kinetic compensation effect during low-temperature oxidation of coal chars. Proc Combust Inst 33:1755–1762
55. Barrie PJ (2012) The mathematical origins of the kinetic compensation effect: 1. The effect of random experimental errors. Phys Chem Chem Phys 14:318–326
56. Barrie PJ (2012) The mathematical origins of the kinetic compensation effect: 2. The effect of systematic errors. Phys Chem Chem Phys 14:327–336